

Timing observations of RRAT J1819-1458 at Urumqi Observatory

A. Esamdin,^{1*} C. S. Zhao,^{1,2} Y. Yan^{1,2}, N. Wang¹, H. Nizamidin³, Z. Y. Liu¹

¹Urumqi Observatory, National Astronomical Observatories, CAS, 40-5 South Beijing Road, Urumqi, 830011, China

²Graduate University of Chinese Academy of Sciences, Beijing 100049, China

³Department of Physics, Xinjiang University, Urumqi, 830046, China

Received ? / Accepted ?

ABSTRACT

We report the timing-analysis results obtained for RRAT J1819-1458 from regular timing observations at 1.54 GHz using the Urumqi 25 m radio telescope between 2007 April to 2008 March. RRAT J1819-1458 is a relatively young and highly magnetized neutron star discovered by its sporadic short bursts in the Parkes Multibeam Pulsar Survey data. In 94 hrs of observation data, we detected a total of 162 dispersed bursts of RRAT J1819-1458 with the signal-to-noise ratios (S/Ns) above 5- σ threshold. Among them, 5 bursts clearly show two-component structure. The S/N of the strongest burst is 13.3. The source's DM measured through our data is 196.0 ± 0.4 pc cm⁻³. The timing position, frequency and its first derivative were determined using standard pulsar timing techniques on the arrival times of these individual bursts. The accuracy of the solved rotating parameters are improved comparing with that in previous publication. Our timing position with 2- σ error is consistent with the position of its X-ray counterpart CXOU J181934.1-145804. The effect of timing noise and the phase fluctuation of the individual short bursts on the timing residuals is briefly discussed. The distribution of the timing residuals is bimodal, which cannot be explained readily by timing irregularity.

Key words: stars: neutron – pulsar: individual: J1819-1458

1 INTRODUCTION

Recently, a remarkable new class of radio transient sources, the “Rotating Radio Transients” (RRATs) was discovered in a search for isolated radio bursts in the Parkes Multibeam Pulsar Survey data (McLaughlin et al. 2006). A total of 11 RRATs have been detected so far; they are characterized by short radio bursts of a typical from 2 to 30 ms duration, and the average time intervals between bursts range from 3 min to 3 hrs. Although the radio bursts of RRATs are sporadic, the timing analysis of the bursts of 10 RRATs indicates that they are likely to be rotating neutron stars with the periods ranging from 0.4 to 7 sec (McLaughlin et al. 2006).

RRAT J1819-1458 is the brightest and the most prolific radio-burster of all 11 RRATs. At 1.4 GHz, the source is characterized by dispersed radio bursts of average duration 3 ms with one burst detected about every 3 min; its dispersion measure (DM) is 196 ± 3 pc cm⁻³; and the peak flux of the brightest burst detected so far is 3.6 Jy. The distance inferred from its DM and position using the free

electron density model of Cordes & Lazio (2004) is about 3.6 kpc. Although the source is not detectable in standard periodicity searches, the analysis of the spacings between the bursts reveals a spin period, $P = 4.263$ s, and a spin period derivative, $\dot{P} = 576 \times 10^{-15}$ s s⁻¹. RRAT J1819-1458 has a characteristic age of 117 kyr, and a relatively high inferred magnetic field strength of 5×10^{13} gauss (McLaughlin et al. 2006).

On the P - \dot{P} diagram, the source is located in the same area occupied by the high magnetic field radio pulsars, which suggests a possible association between RRATs and the magnetars (McLaughlin et al. 2006; for details about magnetar see Woods & Thompson 2006) or the X-ray dim isolated neutron stars (Popov, Turolla & Possenti 2006; for details about XDINSs see Haberl 2004). The *Chandra* observation detected the X-ray counterpart of RRAT J1819-1458 (Reynolds et al. 2006). Lately, using the *XMM-Newton*, McLaughlin et al. (2007) discovered the X-ray pulsations with the period predicted by the timing of radio bursts. The X-ray properties show that RRAT J1819-1458 is a cooling neutron star, and unlikely to be a

* E-mail: aliyi@uao.ac.cn

magnetor (Reynolds et al. 2006; Popov, Turolla & Possenti 2006; McLaughlin et al. 2007; Rutledge 2006).

Based on a study of subpulse modulation of pulsars (Weltevrede, Edwards & Stappers 2006), Weltevrede et al. (2006) note that PSR B0656+14 has very energetic and sporadic radio pulses with the same characteristic as RRATs, and suggest that it could have been identified as a RRAT, were it not so nearby. They point out that these energetic bursts are shown to be unlike giant pulses (e.g. Hankins et al. 2003; Knight et al. 2006), giant micropulses (e.g. Johnston et al. 2001; Johnston & Romani 2002) or the pulses of normal pulsars (e.g. Ritchings 1976; Kramer et al. 2003). Wang, Manchester & Johnston (2007) note RRATs are not directly related to nulling pulsars which are characterized by turning on and off of the pulsations. Although several models have been suggested to explain RRAT phenomenon (Zhang, Gil & Dyks 2007; Li 2006; Cordes & Shannon 2006; Luo & Melrose 2007), the nature of emission of RRATs is as yet unclear.

We observed RRAT J1819-1458 at 1540 MHz by using the Urumqi 25m radio telescope from 10 April 2007 to 29 March 2008. In this paper, we present the timing result of RRAT J1819-1458 based on these observations. The details of the observations are presented in Section 2. The process of burst detection is given in Section 3. The timing process and results are described in Section 4. A brief discussion is given in Section 5. In Section 6 we summarize this study.

2 OBSERVATIONS

The observations of RRAT J1819-1458 have been regularly carried out by using the Urumqi 25-m radio telescope with a dual-channel cryogenic receiver that receives orthogonal linear polarizations at the central observing frequency of 1540MHz. The receiver noise temperature is less than 10 K. After mixing down to an intermediate frequency, the two polarizations are each fed into a filter bank of 128 contiguous channels, each of width 2.5 MHz. The outputs from the channels are then square-law detected, filtered and one-bit sampled at 0.5 ms interval (for details about this system see Wang et al. 2001). The data streams of all 256 channels are written to disk for subsequent off-line processing. The start time of each observation is also recorded to calculate the site arrival time of each pulse of burst.

We detected the isolated dispersed bursts of RRAT J1819-1458 with the S/N above $5\text{-}\sigma$ threshold. The minimum peak flux density of the detected signal is given by

$$S_{min} = \frac{2\alpha\beta k(T_{rec} + T_{spl} + T_{sky})}{\eta A \sqrt{n_p \tau \Delta f}} \quad (1)$$

where $\alpha = 5$ is the threshold signal-to-noise ratio, $\beta = \sqrt{\pi/2}$ is a factor accounting for losses due to 1-bit digitization, k is Boltzmann's constant, T_{rec} , T_{spl} and T_{sky} are receiver, spillover and the sky noise respectively ($T_{rec} + T_{spl} + T_{sky} \sim 32$ K), $n_p = 2$ is number of polarizations summed, $\tau = 0.5$ ms is the sampling interval, $\Delta f = 320$ MHz is the observing bandwidth, $\eta \sim 57\%$ is the efficient of the antenna at 1540 MHz and $A = 490.87\text{m}^2$ is the area of the antenna. We calculated a minimum detectable pulse amplitude of ~ 3.4 Jy for our $5\text{-}\sigma$ detection threshold.

In this work, a total of 47 observations were made within 25 observing sessions from 10 April 2007 to 29 March 2008. The time span of each observation was 2 hrs. The sampling interval of all observations was fixed to 0.5 ms. In total, 94 hrs of observing data were collected in the one-year time span.

3 BURST DETECTION

Radio waves propagating through ionized plasma in the interstellar medium experience a frequency-dependent delay due to the dispersive effects of the plasma. In order to detect short bursts from celestial sources, this frequency-dependent delay has to be removed. The difference in arrival times, Δt (ms), between a pulse received at a high frequency, f_h , and a lower frequency, f_l , is given by

$$\Delta t = 4.148808 \times DM \times \left(\frac{1}{f_l^2} - \frac{1}{f_h^2} \right) \quad (2)$$

where DM is the dispersion measure in pc cm^{-3} , and the frequency values are in GHz. This equation was used to calculate the signal delays in our 128 observing channels of each polarization.

The data processing was performed in several steps in order to detect the dispersed short bursts from RRAT J1819-1458. The observing data were first dedispersed by delaying successive channels in time corresponding to the nominal dispersion measure $DM = 196 \text{ pc cm}^{-3}$, and then searched for all pulses above a $5\text{-}\sigma$ S/N threshold in the dedispersed time series. Secondly, we checked the frequency evolution of these candidate signals. The dispersion is seen as a quadratic sweep across the observing frequency band for the strong bursts detected in this study if two polarizations summed. However, the weaker signals ($S/N \leq 6.5$ in our case) are not strong enough to clearly present this dispersed feature through all frequency channels. We therefore checked if they were broadband by displaying the dedispersed time series in 8 bands each of $16 \times 2.5\text{MHz}$ wide. Thirdly, the dedispersion procedure was performed from zero DM to $DM = 300 \text{ pc cm}^{-3}$ in steps of 1 pc cm^{-3} in order to confirm the dispersion signature in a DM-time space. The S/N of the maximum pulse amplitude was also computed for each DM over a time series of 400 ms centered on the candidate signal. From this analysis, a diagnostic plot (as shown in Fig.1) was generated for each burst candidate. These plots were then subjected to a careful visual inspection to discriminate real bursts from spurious signals.

Fig. 1 shows the diagnostic plots of four bursts detected in this work. Each diagnostic plot contains a DM versus time (top left panel), a S/N versus DM (top right panel) and a dedispersed time series diagram (bottom panel). In DM-time space, a burst is detected as a vertical strip of pulses at multiple DMs around the nominal DM. The strip is gradually broadening and finally smears out with the DM either increasing or decreasing from the nominal DM. The bursts are clearly visible in the DM versus time and the S/N versus DM diagrams with maximum S/N around $DM \sim 196 \text{ pc cm}^{-3}$. Plots (a), (b), and (c) in Fig. 1 show a broad, a narrow and a bimodal burst respectively.

Some of our observing data were contaminated by Radio Frequency Interference (RFI). The frequency-dispersion

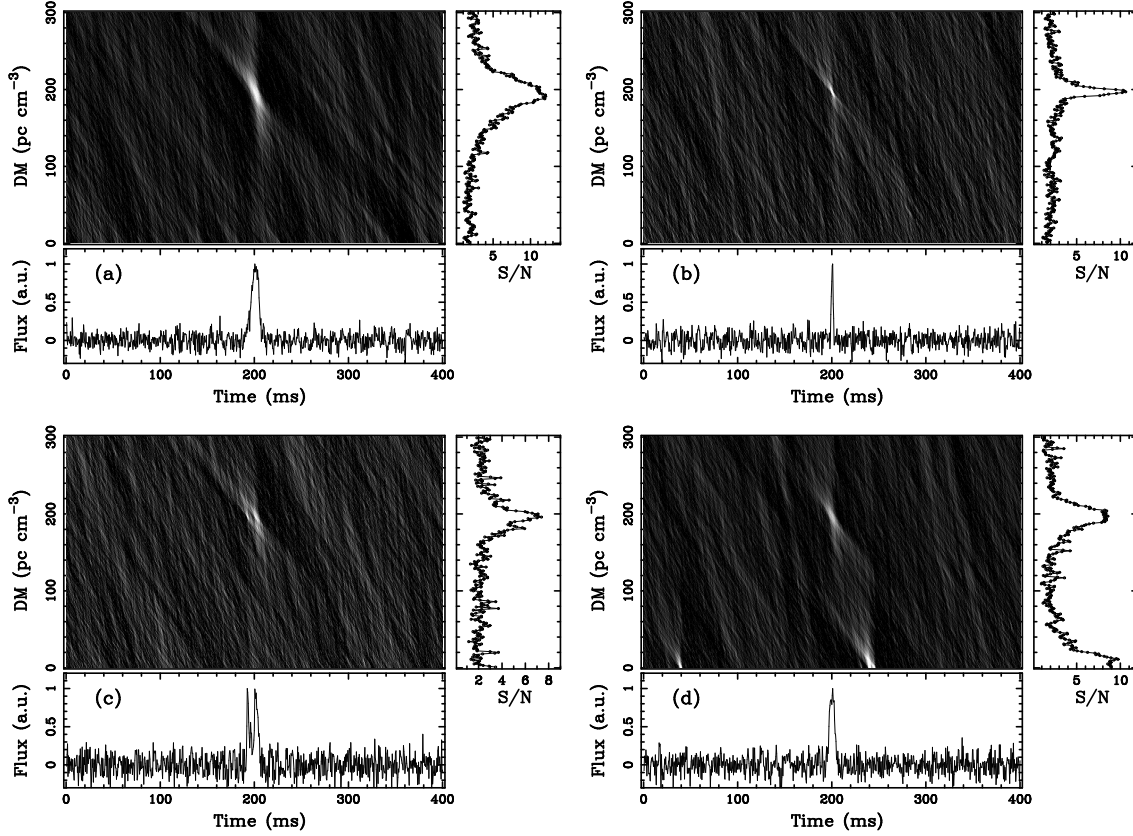


Figure 1. Diagnostic plots show four bursts detected in this work. Each diagnostic plot includes a DM versus time diagram in gray scale (top left panel), a S/N versus DM diagram (top right panel) and a dedispersed burst time series (bottom panel). Dedispersion procedure is performed from zero DM to DM = 300 pc cm⁻³ in steps of 1 pc cm⁻³ to obtain the DM versus time space. The S/N for each DM is calculated for the maximum amplitude in a 400-ms dedispersed time series centered on the candidate pulse. The bursts are clearly visible in the DM versus time and the S/N versus DM diagrams with a maximum S/N near the DM of 196 pc cm⁻³. Plots (a), (b), and (c) present a broad burst, a narrow burst and a bimodal burst respectively. In addition to a real burst signal at the nominal DM, plot (d) also shows two strong pulses of terrestrial radio interference around the zero DM at about 40 ms and 243 ms, respectively.

property of signals may assist to distinguish between signals of celestial origin and locally generated impulsive RFI (Cordes & McLaughlin 2003). As shown in plot (d) in Fig. 1, the two high S/N pulses detected near the zero DM are likely to be impulsive terrestrial interference. The two RFI signals spread from zero DM (at about 40 ms and 243 ms respectively) to several nearby DMs in the DM versus time diagram.

By using the searching method mentioned above, a total of 162 strong bursts, with the S/Ns ranging from 5 to 13.3, are detected in 94 hrs of data. Among them, there are 5 bursts clearly show two-component (bimodal) structure with the separations of the two components ranging from 6 ms to 16.5 ms.

In order to determine the DM of this source through our data, we produce the average S/N versus DM diagram (as shown in Fig. 2) obtained by averaging all S/Ns in each DM step of all 162 bursts. In this case, the dedispersion procedure for each burst is performed from DM=96 to DM = 296 pc cm⁻³ in steps of 0.1 pc cm⁻³. Fig. 2 shows that the peak of the distribution of the average S/Ns is right at DM=196 pc cm⁻³. The rms of S/N fluctuation calculated from the average S/Ns in the DM range from 266 to 296 pc cm⁻³ is 0.032. To determine the DM error, 3- σ level of the S/N fluctuation (~ 0.1) is taken. The DM error measured according

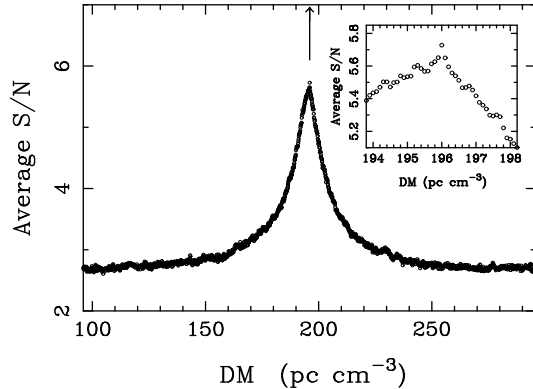


Figure 2. Average S/N versus DM diagram obtained by averaging all S/Ns in each DM step of all 162 bursts. The dedispersion procedure for each burst is performed from DM=96 to DM = 296 pc cm⁻³ in steps of 0.1 pc cm⁻³. The peak of the S/N distribution is right at DM = 196 pc cm⁻³ as indicated by the vertical arrow. The inserted plot shows the variation of the average S/Ns in DM range from 193.8 to 198.2 pc cm⁻³.

to the S/N distribution is ± 0.2 pc cm⁻³. We take twice the value as the error of the DM, and obtain the improved DM = 196.0 ± 0.4 pc cm⁻³ (listed in Table 1).

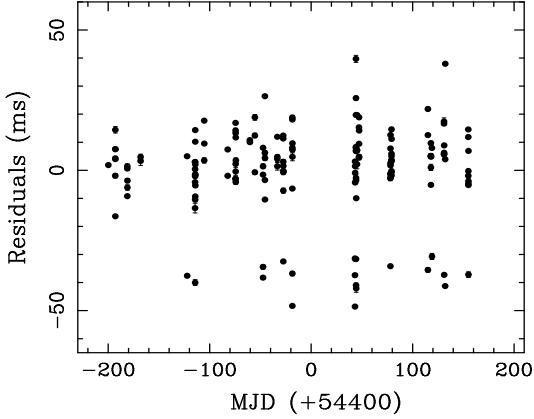


Figure 3. Timing residuals for RRAT J1819-1458 after fitting for the position, rotational frequency and its first derivative. The residuals of 162 individual bursts range from -48.57 ms to 39.71 ms. The rms residual is 16.14 ms. It is about 0.4% of the source’s period.

4 TIMING ANALYSIS AND RESULTS

Mclaughlin et al. (2006) note that RRAT J1819-1458 is only detectable through individual radio bursts. The timing process of the source is therefore slightly different from the standard pulsar timing process in which the times of arrival (TOAs) are determined by fitting a template profile to the observed mean pulse profiles. We measured position, frequency, ν , and frequency first derivatives, $\dot{\nu}$, using standard pulsar timing techniques on the arrival times of individual bursts of the source.

The data are dedispersed (at $DM = 196 \text{ pc cm}^{-3}$) relative to the central observing frequency to form the pulses of the 162 bursts. In our case, TOA of a pulse of burst refers to the pulse’s midpoint which is determined by the center of a Gauss fit to the pulse. However, as mentioned in above section, 5 of the 162 bursts present two component structure. In case of these bimodal-structure bursts, the midpoints of stronger components are used to determine their TOAs. TOAs of the pulses at the telescope are then measured by projecting the start times of the observations to these midpoints. The uncertainties of TOAs are calculated by dividing the half power full widths (W_{50}) of the pulses by their signal to noise ratios. TOAs are processed using the standard TEMPO 2 software package (Hobbs, Edwards & Manchester 2006), which first converts them to solar system barycentric TOAs at infinite frequency using the Jet Propulsion Laboratory Solar-system ephemeris DE405 (Standish 2004), and then performs a least-square fit to determine the model parameters. The position, ν , and $\dot{\nu}$ are quoted for an epoch (MJD 54400) near the midpoint of our data span. The timing residuals, which are the differences between the actual pulse arrival times and those calculated from the fitted model, are then obtained to investigate the phases of bursts and the source’s rotational behavior.

Table 1 lists the best-fitting parameters and their uncertainties, including position, ν and $\dot{\nu}$ at epoch MJD 54400. Uncertainties in the last digit quoted are given in parentheses. These uncertainties are taken to be twice the standard errors obtained from TEMPO2. Table 1 also lists

Table 1. Timing parameters and derived parameters for RRAT J1819-1458. Uncertainties in the last digit quoted are given in parentheses. The uncertainties of timing parameters are twice the standard TEMPO errors.

Parameters	Values
Right Ascension (J2000)	18:19:33.8(4)
Declination (J2000)	-14:58:01(16)
ν (s^{-1})	0.2345648893(7)
$\dot{\nu}$ ($10^{-14} s^{-2}$)	-3.104(2)
DM (pc cm^{-3})	196.0(4)
Epoch (MJD)	54400
Number of TOAs	162
Time span (MJD)	54200.1 – 54555.1
Rms residual (ms)	16.14
τ_c (kyr)	119.81(8)
B_s (gauss)	$4.963(2) \times 10^{13}$
\dot{E} (erg s^{-1})	$2.876(2) \times 10^{32}$
B_{Lc} (gauss)	5.818(2)

the DM determined through our data, the epoch of the period, the number of TOAs included in the timing solution, the MJD range covered and the rms of the post fit timing residuals. We also calculated characteristic age, $\tau_c = P/(2\dot{P})$, the surface dipole magnetic field strength, $B_s = 3.2 \times 10^{19} (P\dot{P})$, the rate of loss in rotational energy, $\dot{E} = 4\pi^2 I \dot{P}/P^3$ (using a standard neutron star moment of inertia $I = 10^{45} \text{ g cm}^2$), and the magnetic field strength at the light cylinder, $B_{Lc} = 9.35 \times 10^5 \dot{P}^{1/2} P^{-5/2}$, as listed in Table 1. These derived parameters are very close to those presented by Mclaughlin et al. (2006). The timing residuals of the 162 bursts are shown in Fig. 3. In this work, the MJD range of the available TOAs is two times longer than for Mclaughlin et al. (2006), and hence the accuracy of the timing solutions has improved correspondingly.

Fig. 4 compares the position obtained in this work with that of published positions. Our fitted position at the reference epoch with J2000 coordinates is: right ascension = $18^h 19^m 33.8 \pm 0^s.4$ and declination = $-14^h 58^m 01^s \pm 16$ (J2000). This is consistent with the more accurate position for the X-ray counterpart (CXOU J181934.1-145804) published in Reynolds et al. (2006) and with the timing position reported in Mclaughlin et al. (2006) assuming 2σ uncertainties for the values quoted in that paper. Long-term observations are necessary to acquire more precise timing position of the source.

As shown in Fig.3, the measured timing residuals range from - 48.57 ms to 39.71 ms. The rms residual (16.14 ms) is about 0.4% of the source’s period. RRAT J1819-1458 is a relatively young neutron star which is very likely to show a significant timing irregularity. The residuals of single-pulse timing are contributed both by the timing irregularity and by the modulation of pulse phase in the radiation window. It is therefore difficult to discriminate the intrinsic rotating irregularity (especially the timing noise) from the phase modulation through the timing residuals of the sporadic individual bursts. However, Fig.3 shows that no significant glitch, which would produce continually growing (negative) arrival-

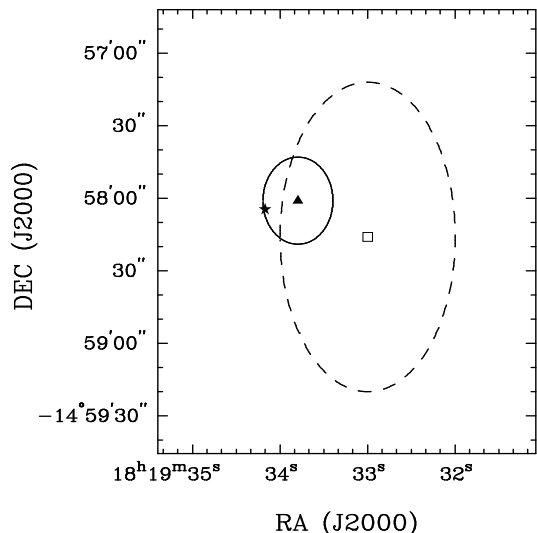


Figure 4. A comparison between the timing position obtained in this work (filled triangle) with that reported in Mclaughlin et al. (2006) (open square) and with the position of CXOU J181934.1-145804 (Reynolds et al. 2006) (star). The error ellipses indicate the 2- σ errors of the standard tempo uncertainties.

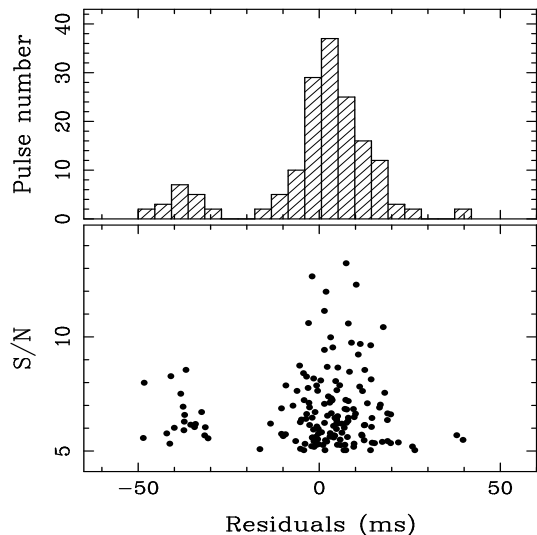


Figure 5. Histogram of residuals (top panel), and the S/N versus residuals diagram (bottom panel). The distribution of the timing residuals of 162 bursts shows a bimodal structure, peaked at about -37 ms and 3 ms. This may indicate a possible weak preceding component 40 ms ahead of the main component in the radiation window of RRAT J1819-1458. The S/Ns of the bursts range from 5 to 13.3.

time residuals, is detected in the one year of rotating history of the source.

Fig. 5 presents a histogram of residuals and a S/N versus residual diagram. As shown in Fig. 3 and Fig. 5, the residual distribution of these strong bursts is clearly bimodal, peaked at about -37 ms (leading peak) and 3 ms (main peak) respectively. The pulse number detected around the leading peak and the main peak are 18 and 144 respectively. The implication of the distribution of the timing residuals is discussed in following section.

5 DISCUSSION

In order to estimate a possible contribution of stochastic timing noise to the timing residuals, we calculated the cumulative phase contributed by timing noise over time interval of our observations (~ 355 days). If we express the rotation frequency as a Taylor series, the pulse phase at time t is given by

$$\phi = \phi_0 + \nu t + \frac{1}{2}\dot{\nu}t^2 + \frac{1}{6}\ddot{\nu}t^3 \dots \quad (3)$$

where ϕ_0 is the phase in cycles at time $t = 0$. The fourth term in this equation can be used to estimate the cumulative phase contributed by stochastic timing noise over time interval t . We therefore carried out a timing solution with the second frequency derivative $\ddot{\nu}$ included, and detected no significant decrease of the rms residual. Because $|\ddot{\nu}| < 2\sigma_{\ddot{\nu}}$ in our case, following Arzoumanian et al. (1994), we quoted an upper limit of the cumulative phase (δ_t) as

$$\delta_t < \frac{1}{6\nu}(2\sigma_{\ddot{\nu}})t^3 \quad (4)$$

where $\nu = 0.23456$ is the rotating frequency, $\sigma_{\ddot{\nu}} = 1.19 \times 10^{-24}$ is the formal uncertainty of the second frequency derivative, and $t \sim 30672000$ s is the time interval over our observations. We obtained the cumulative phase, $\delta_t < 50$ ms, in a one year time span.

Although the cumulative phase reaches 50 ms in a one year duration, the result of a fitting for ν and $\dot{\nu}$ to a simple rotating model with the $\ddot{\nu}$ included shows that the rms residual is less than 2 ms. The rms of timing residuals in Table 1 is much larger than that contributed by the stochastic timing noise expected for this source over one year. If we take a typical duty cycle value of 3% of normal pulsars, the burst-phase span of a 4.26 sec pulsar is expected to be about 130 ms. For these reasons, we may note that the residuals in Fig. 3 are strongly dominated by random fluctuations in the burst phases, and can be good representations of the phases of the individual bursts in the source's radiation window.

The bimodal distribution of the residuals (as shown in Fig. 5) cannot be explained readily by timing irregularity, and may indicate the possible existence of a more sporadic burst activity in the longitudinal region preceding the main radiation region. However, the number of detected bursts is not yet sufficient to make this a firm conclusion. More observations and an accurate phase alignment are needed to obtain a reliable luminosity distribution of the radiation window.

As shown in Table 1, RRAT J1819-1458 is a relatively young pulsar with a long spin period and a high B_s . In fact, there are only 16 pulsars in ANTF Pulsar Catalog with the measured B_s values higher than that of this source. It has a modest \dot{E} and a low B_{Lc} in the known pulsar population. The unusual radio emission and the detection of X-ray pulsation of RRAT J1819-1458 make it a very interesting object. Its sporadic radio activity may have similar mechanism with one of the two known radio-emission phenomena, i.e. giant-pulse emission in some pulsars (e.g. Hankins et al. 2003; Knight et al. 2006) or the very sporadic strong pulses detected in PSR B0656+14 (Weltevredre et al. 2006). The known giant-pulse emitters have very high values of B_{Lc} ($> 10^5$ gauss) and \dot{E} ($\sim 10^{36-38}$) which are suggested to be indicators of giant-pulse

emissivity (Cognard et al. 1996; McLaughlin & Cordes 2003; Knight et al. 2006). Therefore, the low B_{Lc} and \dot{E} of RRAT J1819-1458 is against the suggestion of giant-pulse origin of its radio bursts (McLaughlin et al. 2006, 2007). The characteristic ages of PSR B0656+14 and RRAT J1819-1458 are similar, and the X-ray pulsation characteristics of RRAT J1819-1458 seems to be similar with that of PSR B0656+14 (McLaughlin et al. 2007). However, we should note that the two sources have very different spin period, B_s and \dot{E} . The anomalous X-ray pulsars (AXPs) have very high values of B_s . Therefore, the transient radio emission detected in AXPs XTE J1810-197 and 1E 1547.0-5408 (Camilo et al. 2006, 2007) may also have a similar mechanism with the radio emission of this high- B_s RRAT. However, the radio emission characteristics of the two AXPs are quite different from that of RRAT J1819-1458 (McLaughlin et al. 2006). By studying the X-ray properties, McLaughlin et al. (2007) note that RRAT J1819-1458 could be a transition object between the pulsar and magnetar. More studies are needed to determine the reason of the source's unusual radio behavior. A study of individual-burst properties of RRAT J1819-1458 mainly based on the bursts presented in this paper will be reported in a subsequent paper.

6 SUMMARY

We have carried out timing observations of RRAT J1819-1458 by using the Urumqi 25 m radio telescope at a center frequency of 1.54 GHz. A total of 47 observations were made in 25 sessions from 10 April 2007 to 29 March 2008. In total 162 strong bursts, with $S/N \geq 5$, were detected through a careful burst-detection processing. 5 bimodal bursts, with the component separations ranging from 6 ms to 16.5 ms, were noted. We obtained a more precise $DM = 196.0 \pm 0.4$ pc cm $^{-3}$ from our data. We have presented the improved timing position, ν and $\dot{\nu}$ for RRAT J1819-1458 based on these bursts using standard pulsar timing techniques on the arrival times of individual bursts. The location of the X-ray counterpart (CXOU J181934.1-145804) is now within 2σ error ellipse of our timing position.

No evidence of significant glitch and timing noise were found in the one year of rotating history of this source, likely due to the phase modulation of the sparse individual pulses of bursts within its radiation windows. Continued monitoring is needed to investigate its rotating irregularity. We found a bimodal distribution of the timing residuals, which may suggest a possible two-component structure of the source's radiation window, with a more sporadic component leading the main one. However, more observations are also necessary to confirm this conclusion.

ACKNOWLEDGMENTS

We thank the reviewer for the very helpful comments. The authors are supported by the National Natural Science Foundation of China (NSFC) under grant 10573026 and 10778631, the program of the Light in China's Western Region (LCWR) under grant. LHXZ200602, and the Knowledge Innovation Program of the Chinese Academy of Science under grant KJCX2-YW-T09.

REFERENCES

- Arzoumanian Z., Nice D. J., Taylor J. H., Thorsett S. E., 1994, *ApJ*, 422, 671
- Camilo F., Ransom S. M., Halpern J. P., Reynolds J., 2007, *ApJ*, 666, L93
- Camilo F., Ransom S. M., Halpern J. P., Reynolds J., Helfand D. J., 2006, *Nature*, 442, 892
- Cognard I., Shrauner J. A., Taylor J. H., Thorsett S. E., 1996, *ApJ*, 457, L81
- Cordes J. M., Lazio T. J. W., 2004, *ASPC*, 317, 211
- Cordes J. M., McLaughlin M., 2003, *ApJ*, 596, 1142
- Cordes J. M., Shannon R. M., 2006, *astro-ph/0605145*
- Haberl F., 2004, *AdvSpR*, 33, 638
- Hankins T. H., Kern J. S., Weatherall J. C., Eilek J. A., 2003, *Nature*, 422, 141
- Hobbs G. B., Edwards R. T., Manchester R. N., 2006, *MNRAS*, 369, 655
- Johnston S., Romani R., 2002, *MNRAS*, 332, 109
- Johnston S., van Straten W., Kramer M., Bailes M., 2001, *ApJ*, 549, L101
- Knight H. S., Bailes M., Manchester R. N., Ord S. M., Jacoby B. A., 2006, *ApJ*, 640, 941
- Kramer M., Karastergiou A., Gupta Y., Johnston S., Bhat N. D. R., Lyne A. G., 2003, *A&A*, 407, 655
- Li X. D., 2006, *ApJ*, 646, L139
- Luo Q., Melrose D., 2007, *MNRAS*, 378, 1481
- McLaughlin M. A., Cordes J. M., 2003, *ApJ*, 596, 982
- McLaughlin M. A., Lyne A. G., Lorimer D. R., Kramer M., Faulkner A. J., Manchester R. N., Cordes J. M., Camilo F., Possenti A., Stairs I. H., Hobbs G., D'Amico N., Burgay M., O'Brien J. T., 2006, *Nature*, 439, 817
- McLaughlin M. A., Rea N., Gaensler B. M., Chatterjee S., Camilo F., Kramer M., Lorimer D. R., Lyne A. G., Israel G. L., Possenti A., 2007, *ApJ*, 670, 1307
- Popov S. B., Turolla R., Possenti A., 2006, *MNRAS*, 369, 23
- Reynolds S. P., Borkowski K. J., Gaensler B. M., Rea N.; McLaughlin M., Possenti A., Israel G., Burgay M., Camilo F., Chatterjee S., Kramer M., Lyne A. G., Stairs I., 2006, *APJ*, 639, 71
- Ritchings R. T., 1976, *MNRAS*, 176, 249
- Rutledge R. E., 2006, *astro-ph/0609200*
- Standish, E. M. 2004, *A&A*, 417, 1165.
- Wang N., Manchester R. N., Johnston S., 2007, *MNRAS*, 377, 1383
- Wang N., Manchester R. N., Zhang J., Wu X. J., Yusup A., Lyne A. G., Cheng K. S., Chen M. Z., 2001, *MNRAS*, 328, 855
- Weltevredre P., Edwards R. T., Stappers B. W., 2006, *A&A*, 445, 243
- Weltevredre P., Stappers B. W., Rankin J. M., Wright G. A. E., 2006, *ApJ*, 645, 149
- Woods P. M., Thompson C., 2006, in Lewin W. H. G., van der Klis M., eds, *Compact stellar X-ray sources*. Cambridge Univ. Press, Cambridge, 547
- Zhang B., Gil J., Dyks J., 2007, *MNRAS*, 374, 1103